

## Proton inelastic scattering to continuum studied with antisymmetrized molecular dynamics

Eiji I. Tanaka, Akira Ono, Hisashi Horiuchi, Tomoyuki Maruyama\*, and Andreas Engel  
*Department of Physics, Kyoto University, Kyoto 606-01, Japan*

### Abstract

Intermediate energy (p, p'x) reaction is studied with antisymmetrized molecular dynamics (AMD) in the cases of  $^{58}\text{Ni}$  target with  $E_p = 120$  MeV and  $^{12}\text{C}$  target with  $E_p = 200$  and 90 MeV. Angular distributions for various  $E_{p'}$  energies are shown to be reproduced well without any adjustable parameter, which shows the reliability and usefulness of AMD in describing light-ion reactions. Detailed analyses of the calculations are made in the case of  $^{58}\text{Ni}$  target and following results are obtained: Two-step contributions are found to be dominant in some large angle region and to be indispensable for the reproduction of data. Furthermore the reproduction of data in the large angle region  $\theta \gtrsim 120^\circ$  for  $E_{p'} = 100$  MeV is shown to be due to three-step contributions. Angular distributions for  $E_{p'} \gtrsim 40$  MeV are found to be insensitive to the choice of different in-medium nucleon-nucleon cross sections  $\sigma_{NN}$  and the reason of this insensitivity is discussed in detail. On the other hand, the total reaction cross section and the cross section of evaporated protons are found to be sensitive to  $\sigma_{NN}$ . In the course of the analyses of the calculations, comparison is made with the distorted wave approach.

25.40.Ep, 24.50.+g, 24.10.-i

Typeset using REVTeX

---

\*Present address: Advanced Science Research Center, Japan Atomic Energy Research Institute, Tokai-mura, Ibaraki-ken 319-11, Japan.

## I. INTRODUCTION

Nucleon inelastic scattering to continuum at intermediate energies has been extensively studied, through which our understanding of pre-equilibrium processes in the scattering has much advanced. Among many kinds of theoretical investigations including the exciton model [1,2] and other multi-step reaction theories [3–5], the intra-nuclear cascade model (INC) [6,7] has served as an important approach since the activation of many degrees of freedom in pre-equilibrium processes is complicated compared to the compound-nucleus reaction process with full equilibration. Because the original INC model has several drawbacks such as the absence of the attractive interaction among nucleons, many kinds of modifications have been introduced into the INC model.

Recently, besides INC and its modified versions, new types of transport theories (or microscopic simulation theories) like BUU (Boltzmann-Uehling-Uhlenbeck) [8], QMD (quantum molecular dynamics) [9,10], and AMD (antisymmetrized molecular dynamics) [11,12] have been developed in order to investigate complicated reaction processes of heavy-ion collisions at intermediate and high energies. These new types of transport theories can describe the self-consistent mean field of the system which changes with time depending on the stage of the reaction process. These theories are, of course, also applicable to light-ion reactions including the nucleon inelastic scattering to continuum.

We think that QMD and AMD approaches to reactions induced by light ions and also hadrons and leptons are especially important. These molecular dynamics models can describe dynamical production processes of fragments and hence they can provide us with a unified theoretical description of two different kinds of reaction processes, namely processes of the type of light-ion physics and those of the type of heavy-ion physics. Nucleon inelastic scattering to continuum belongs to the former type and fragmentation reaction to the latter type.

In this paper we study proton inelastic scattering to continuum at intermediate energies by the use of the AMD model. The AMD model is a new transport theory and has already proved to be very successful in describing heavy-ion collisions at medium energies [12–18]. AMD describes the total system with a Slater determinant of nucleon wave packets and hence it has quantum mechanical character, which has been demonstrated in the ability of treating shell effects in the dynamical formation of fragments. Furthermore it has been shown that ground-state wave functions of colliding nuclei given by the AMD model are realistic and reproduce many spectroscopic data very well [19–21]. We report in this paper the study of (p, p'x) reaction in the cases of  $^{58}\text{Ni}$  target with  $E_p = 120$  MeV and  $^{12}\text{C}$  target with  $E_p = 200$  and 90 MeV. We show that the angular distributions are well reproduced by AMD without any adjustable parameter. This shows the reliability and usefulness of AMD in treating light-ion reactions. We make detailed analyses of the calculations in the case of  $^{58}\text{Ni}$  target in the following way: We decompose the calculated cross sections into the contributions coming from different steps in order to study magnitudes of multi-step contributions. Two-step contributions are shown to be dominant in some large angle region and to be indispensable for the reproduction of data. Furthermore the reproduction of data in the large angle region  $\theta \gtrsim 120^\circ$  for  $E_{p'} = 100$  MeV is shown to be due to three-step contributions. Angular distributions for  $E_{p'} \gtrsim 40$  MeV are shown to be insensitive to the choice of different in-medium nucleon-nucleon cross sections  $\sigma_{NN}$  and the reason of this

insensitivity is discussed in detail. On the other hand, the total reaction cross section and cross section of evaporated protons are shown to be sensitive to  $\sigma_{NN}$ . In discussing the calculated results we make comparison with the results obtained with the semi-classical distorted-wave approach of Ref. [22].

The organization of this paper is as follows: In Sec. II we explain the AMD framework, the adopted effective two-nucleon force, and three choices of in-medium nucleon-nucleon cross section  $\sigma_{NN}$ . A detailed explanation of the definition of the step number of reaction process is also given. In Sec. III we give the comparison with experiments of the calculated angular distributions at various  $E_{p'}$  energies. Here the decomposition of the cross sections into multi-step contributions is also made. In Sec. IV we make detailed analysis of the dependence of the calculation on the different choice of  $\sigma_{NN}$ . Finally in Sec. V we give the summary.

## II. FORMULATION

### A. AMD

The framework of AMD (antisymmetrized molecular dynamics) was described in detail in Ref. [12] and hence we here explain only the outline of the AMD theory.

In AMD, the wave function of  $A$ -nucleon system is described by a Slater determinant  $|\Phi(Z)\rangle$ ,

$$|\Phi(Z)\rangle = \frac{1}{\sqrt{A!}} \det[\varphi_j(k)], \quad \varphi_j = \phi_{\mathbf{z}_j} \chi_{\alpha_j} \quad (1)$$

where  $\chi$  stands for the spin-isospin function and  $\alpha_j$  represents the spin-isospin label of the  $j$ -th single particle state,  $\alpha_j = p \uparrow, p \downarrow, n \uparrow, \text{ or } n \downarrow$ .  $\phi_{\mathbf{z}_j}$  is the spatial wave function of the  $j$ -th single-particle state which is a Gaussian wave packet,

$$\begin{aligned} \langle \mathbf{r} | \phi_{\mathbf{z}_j} \rangle &= \left(\frac{2\nu}{\pi}\right)^{3/4} \exp\left[-\nu\left(\mathbf{r} - \frac{\mathbf{Z}_j}{\sqrt{\nu}}\right)^2 + \frac{1}{2}\mathbf{Z}_j^2\right], \\ \mathbf{Z}_j &= \sqrt{\nu}\mathbf{D}_j + \frac{i}{2\hbar\sqrt{\nu}}\mathbf{K}_j, \end{aligned} \quad (2)$$

where the width parameter  $\nu$  is treated as time-independent in the present work. We take  $\nu=0.16 \text{ fm}^{-2}$  in the calculation in this paper. Here  $\mathbf{Z}_j$  is the complex vector whose real and imaginary parts,  $\mathbf{D}_j$  and  $\mathbf{K}_j$ , are the spatial and momentum centers of the packet, respectively.

The time developments of the coordinate parameters,  $Z = \{\mathbf{Z}_j (j = 1, 2, \dots, A)\}$ , are determined by two processes. One is the time development determined by the time-dependent variational principle;

$$\delta \int_{t_1}^{t_2} dt \frac{\langle \Phi(Z) | (i\hbar \frac{d}{dt} - H) | \Phi(Z) \rangle}{\langle \Phi(Z) | \Phi(Z) \rangle} = 0, \quad (3)$$

which leads to the equation of motion for  $Z$ ,

$$\begin{aligned}
i\hbar \sum_{j\tau} C_{k\sigma,j\tau} \frac{d}{dt} Z_{j\tau} &= \frac{\partial}{\partial Z_{k\sigma}^*} \frac{\langle \Phi(Z) | H | \Phi(Z) \rangle}{\langle \Phi(Z) | \Phi(Z) \rangle}, \\
C_{k\sigma,j\tau} &\equiv \frac{\partial^2}{\partial Z_{k\sigma}^* \partial Z_{j\tau}} \ln \langle \Phi(Z) | \Phi(Z) \rangle,
\end{aligned} \tag{4}$$

where  $\sigma, \tau = x, y, z$ .

During the dynamical reaction stage, the total system can be separated into several isolated nucleons and fragments. Since the wave functions of the center-of-mass motion of these isolated nucleons and fragments are Gaussian wave packets, each of these isolated particles carries spurious zero-point energy of its center-of-mass motion. The total amount of the spurious energy of center-of-mass motion can be expressed as a function of  $Z$  [12,14], which we denote as  $E_{\text{sprs}}(Z)$ . The actual Hamiltonian we use in the above equation of motion (Eq. (4)) is, therefore, given by  $\langle \Phi(Z) | H | \Phi(Z) \rangle / \langle \Phi(Z) | \Phi(Z) \rangle - E_{\text{sprs}}(Z)$ .

The second process which determines the time development of the system is the stochastic two-nucleon collision process. We incorporate this process in a similar way as it is done in QMD by introducing the physical nucleon coordinates  $\{\mathbf{W}_j\}$ , mimicking the time-dependent cluster model (TDCM) [23], as

$$\begin{aligned}
\mathbf{W}_j &= \sqrt{\nu} \mathbf{R}_j + \frac{i}{2\hbar\sqrt{\nu}} \mathbf{P}_j \equiv \sum_{k=1}^A (\sqrt{Q})_{jk} \mathbf{Z}_k, \\
Q_{jk} &\equiv \frac{\partial}{\partial (\mathbf{Z}_j^* \cdot \mathbf{Z}_k)} \ln \langle \Phi(Z) | \Phi(Z) \rangle.
\end{aligned} \tag{5}$$

Here it should be noted that, due to the antisymmetrization,  $\mathbf{D}_j$  and  $\mathbf{K}_j$  of  $\mathbf{Z}_j$  do not represent the position and momentum of  $j$ -th nucleon, respectively. When physical nucleon positions  $\mathbf{R}_j$  and  $\mathbf{R}_k$  become close each other, these  $j$ -th and  $k$ -th nucleons can make stochastic two-nucleon collisions. Let initial  $\mathbf{W}_j$  and  $\mathbf{W}_k$  be changed into final  $\mathbf{W}'_j$  and  $\mathbf{W}'_k$  by a two-nucleon collision. In order to continue the calculation of time development of the system wave function after this collision, we need to back-transform  $\{\mathbf{W}_1, \dots, \mathbf{W}'_j, \dots, \mathbf{W}'_k, \dots, \mathbf{W}_A\}$  into  $\{\mathbf{Z}'_1, \mathbf{Z}'_2, \dots, \mathbf{Z}'_A\}$ . However, in general, the back-transformation from  $W = \{\mathbf{W}_j (j = 1, \dots, A)\}$  to  $Z = \{\mathbf{Z}_j (j = 1, \dots, A)\}$  does not always exist. When the back-transformation does not exist, we regard that the two-nucleon collision is Pauli-blocked.  $W$  is defined to be in Pauli-forbidden region if it cannot be back-transformed to any  $Z$ . The notion of the Pauli-forbidden region defined above is an extension of that of TDCM [23]. AMD without stochastic two-nucleon collisions is the same as FMD (Fermionic Molecular Dynamics) [24], and FMD is a special case of TDCM [25,23] where every cluster is composed of a single nucleon.

The full procedure of the AMD description of the nuclear reaction consists of three major steps: The first step is the initialization, namely the construction of the wave functions of the ground states of colliding nuclei. The initialization is made by the use of the frictional cooling method [11,19–21]. It has been checked that wave functions given by AMD are realistic and reproduce many spectroscopic data very well. The second step is the calculation of dynamical collision stage by the equation of motion and stochastic two-nucleon collisions. The final step is the calculation of the statistical decay of primordial fragments. Primordial fragments mean the fragments which are present when the dynamical stage of the reaction

has finished. These fragments are not in their ground states but are excited, and they decay through evaporation with a long time scale. In this paper, the switching time from the dynamical stage to the evaporation stage was chosen to be 150 fm/c. Statistical decays of fragments were calculated with the code of Ref. [26] which is similar to the code of Pühlhofer [27].

## B. Effective force and in-medium nucleon-nucleon cross sections

As the effective two-nucleon force, we adopt the Gogny force [28] which has been successfully used in studying heavy-ion reactions with AMD [14,15]. The Gogny force consists of finite-range two-body force and density-dependent zero-range repulsive force. This force gives a momentum-dependent mean field which reproduces well the observed energy dependence of the nucleon optical potential up to about 200 MeV. The nuclear matter EOS given by this force is soft with the incompressibility  $K = 228$  MeV. Corresponding to the choice of Gogny force, the calculational formula of the total spurious center-of-mass energy  $E_{\text{sprs}}(Z)$  is taken to be the same as Ref. [14] in the case of  $^{12}\text{C}$  target, while in the case of  $^{58}\text{Ni}$  target the value of the  $T_0$  parameter in the formula of  $E_{\text{sprs}}(Z)$  is changed into 8.70 MeV leaving other parameters unchanged. The binding energies of  $^{12}\text{C}$  and  $^{58}\text{Ni}$  are calculated to be 92.6 MeV and 507.6 MeV, respectively, while the observed values are 92.2 MeV and 506.5 MeV, respectively. The r.m.s. radii of  $^{12}\text{C}$  and  $^{58}\text{Ni}$  are calculated to be 2.55 fm and 3.85 fm, respectively, which are reasonable.

As the in-medium nucleon-nucleon cross section  $\sigma_{NN}$ , we adopt the following three different ones, case-1, case-2, and case-3: Case-1  $\sigma_{NN}$  including its angular distribution is the same as the  $\sigma_{NN}$  used in Ref. [14] and is given as  $\sigma_{NN} = \min\{\sigma_{NN}^H, \sigma_{NN}^L\}$ . Here  $\sigma_{NN}^H$  defines the cross section for the high energy region and is the same as the free cross section which is parametrized as

$$\begin{aligned}\sigma_{pn}^H &= \max\{13335(E/\text{MeV})^{-1.125}, 40\} \text{ mb}, \\ \sigma_{pp}^H &= \sigma_{nn}^H = \max\{4445(E/\text{MeV})^{-1.125}, 25\} \text{ mb}.\end{aligned}\quad (6)$$

where  $E$  is the laboratory energy. On the other hand,  $\sigma_{NN}^L$  defines the cross section for the low energy region. It is density-dependent and is given as

$$\begin{aligned}\sigma_{pn}^L &= \sigma_{pp}^L = \sigma_{nn}^L \\ &= \frac{100 \text{ mb}}{1 + E/(200\text{MeV}) + C \min\{(\rho/\rho_0)^{1/2}, 1\}}, \\ C &= 2.\end{aligned}\quad (7)$$

where  $\rho_0$  is the normal density,  $\rho_0 = 0.17 \text{ fm}^{-3}$ . The center-of-mass angular distribution of  $pp$  and  $nn$  collisions is taken to be isotropic while that of  $pn$  collisions is given as

$$\begin{aligned}\frac{d\sigma_{pn}}{d\Omega} &\propto 10^{-\alpha(\pi/2-|\theta-\pi/2|)}, \\ \alpha &= \frac{2}{\pi} \max\{0.333 \ln(E/(1\text{MeV})) - 1, 0\}.\end{aligned}\quad (8)$$

Case-2  $\sigma_{NN}$  is the same as case-1  $\sigma_{NN}$  except that  $C$  of  $\sigma_{NN}^L$  is taken to be  $C = 0$  instead of  $C = 2$ . Hence case-2  $\sigma_{NN}$  is not dependent on density. Case-3  $\sigma_{NN}$  including its angular distribution is the same as the cross section adopted in Ref. [22]. It is just the free cross section and its parametrization is taken from Ref. [6] as follows;

$$\begin{aligned}\sigma_{pn} &= \left( \frac{34.10}{\beta^2} - \frac{82.2}{\beta} + 82.2 \right) \text{ mb}, \\ \sigma_{pp} = \sigma_{nn} &= \left( \frac{10.63}{\beta^2} - \frac{29.92}{\beta} + 49.9 \right) \text{ mb}, \\ \beta &= \frac{v}{c} = \sqrt{\frac{2E}{mc^2}}.\end{aligned}\tag{9}$$

The center-of-mass angular distribution is taken from Ref. [29], where  $pp$  and  $nn$  collisions is isotropic while that of  $pn$  collisions for  $40 \text{ MeV} < E < 280 \text{ MeV}$  is given as

$$\frac{d\sigma_{pn}}{d\Omega} \propto \begin{cases} A_1(E) + B_1(E)(\cos \theta)^3, & \text{for } 0 \leq \theta \leq \pi/2 \\ A_1(E) + B_2(E)(\cos \theta)^4, & \text{for } \pi/2 \leq \theta \leq \pi \end{cases}\tag{10}$$

with values of  $A_1(E)$ ,  $B_1(E)$ , and  $B_2(E)$  being shown in Table I. The  $pn$  collisions below 40 MeV is taken to be isotropic.

In this paper we study  $^{12}\text{C}(p, p'x)$  by using only case-1  $\sigma_{NN}$ , while we apply all the three kinds of  $\sigma_{NN}$  to the study of  $^{58}\text{Ni}(p, p'x)$ .

### C. Step number of reaction process

Here for the sake of later discussion of multi-step processes, we define the number of steps in our AMD approach. What we need is to determine for each out-coming proton the step number of the reaction process. The step number should be defined as the number of collisions which have contributed in emitting the nucleon. If an outcoming proton originates from the decay of some primordial fragment, the process which this proton has experienced is a compound-nucleus process and we need not to define the step number; namely the step number is concerned only with protons which are emitted dynamically.

The step numbers are defined and calculated in the following way. We put a label to every nucleon so that the label of the incident proton is 1. Let us consider the first collision of the incident proton with a target nucleon with label  $k$ . After the first collision, each of the two nucleons 1 and  $k$  may further make collisions with other target nucleons. We put ordering numbers to all these successive collisions beginning with the first collision. We call the ordering number of collision the collision index. The collision index of the first collision is No.1. Just after the first collision, we let each nucleon  $i$  of the total system carry its respective set  $C_i(1)$  composed of related previous collision indices. The sets  $C_1(1)$  and  $C_k(1)$  of the two nucleons 1 and  $k$  are  $C_1(1) = C_k(1) = \{\text{No.1}\}$  but the sets  $C_i(1)$  of other nucleons ( $i \neq 1, k$ ) are all null, namely  $C_i(1) = \emptyset$  ( $i \neq 1, k$ ). One of the nucleons 1 and  $k$  can make the collision with collision index No.2. Let us consider the case that the nucleon  $k$  makes the No.2 collision with a nucleon  $j$ . Then, just after the No.2 collision we let the nucleons  $k$  and  $j$  carry not the old sets  $C_k(1) = \{\text{No.1}\}$  and  $C_j(1) = \emptyset$  but new sets

$C_k(2) = C_j(2) = \{\text{No.1, No.2}\}$ . However, the sets  $C_i(2)$  of other nucleons than  $k$  and  $j$  after the No.2 collision are made unchanged, namely  $C_i(2) = C_i(1)$  for  $i \neq k, j$ . In general, if a nucleon  $m$  makes the No. $p$  collision with a nucleon  $n$ , the new sets after the No. $p$  collision are

$$\begin{aligned} C_m(p) &= C_n(p) = C_m(p-1) \cup C_n(p-1) \cup \{\text{No.}p\}, \\ C_i(p) &= C_i(p-1) \quad \text{for } i \neq m, n. \end{aligned} \tag{11}$$

Note that the double counting of the same collision index is to be avoided in constructing new sets  $\{C_i(p)\}$  from old sets  $\{C_i(p-1)\}$ .

What is important in the above rule is that we only consider two-nucleon collisions which occur successively starting with the first collision of the incident proton as we explained above in time order. We give collision indices only to these two-nucleon collisions and we call them indexed collisions. Any other two-nucleon collisions which are not induced by the first collision of the incident proton have no collision index and are called non-indexed collisions. Non-indexed collisions play no role in constructing the sets  $\{C_i(p)\}$ . For example, the set  $C_i(p)$  of a nucleon  $i \neq 1$  remains to be a null set for any  $p$  if this nucleon  $i$  is not involved at all in any indexed collision, even when it experiences many non-indexed collisions.

Thus the set  $C_i(p)$  is a set composed of all the indexed collisions that have had influence on the  $i$ -th nucleon at the moment just after the No. $p$  collision. If the total number of collision indices contained in  $C_i(p)$  is  $N$ , the nucleon  $i$  after the No. $p$  collision is regarded as having a step number  $N$ . Especially when an outgoing nucleon has a step number  $N$ , this nucleon is defined to be due to  $N$ -step process.

In Fig. 1 we give two illustrative examples of multi-step process. In both cases (i) and (ii) of this figure, the nucleon (a) is the incident proton and collision points are labeled by collision indices 1, 2, ... instead of No.1, No.2, ... In the case of (i), both of outgoing nucleons (b) and (c) carry the same set of collision indices  $\{1, 2, 3\}$  and hence are three-step nucleons. In the case of (ii), the nucleon (b) carries a set of collision indices  $\{1, 2, 3\}$ , and hence is a three-step nucleon, while the nucleon (c) carrying a set of collision indices  $\{1, 2, 3, 4\}$  is a four-step nucleon. We should note here that the three-step nucleons (b) and (c) in the case of (i) are formed as the result of a different type of collision process from the three-step nucleon (b) in the case of (ii). In the case of (i), the three-step nucleons are formed by the collision of a two-step nucleon with a zero-step nucleon. On the other hand, in the case of (ii), the three-step nucleon is produced by a collision of a two-step nucleon with a one-step nucleon. In general, the type of collision process in the case of (i), namely the collision of a two-step nucleon with a zero-step nucleon, is more frequent in producing a three-step nucleon.

Recently Kawai and his collaborators have developed a semi-classical distorted wave model of nucleon inelastic scattering to continuum [30–32]. In this model, the first and second Born terms are shown to correspond to one-collision and two-collision processes in the INC model and are called one-step and two-step processes, respectively. Our above definition of one-step and two-step processes is clearly the same as that in this semi-classical distorted wave model. We further expect that our  $N$ -step process higher than two-step process will be proved to correspond to the  $N$ -th Born term if their semi-classical distorted wave model is extended to higher Born terms.

### III. COMPARISON WITH DATA

We have studied  $^{12}\text{C}(p, p'x)$  at  $E_p = 200$  and  $90$  MeV, and  $^{58}\text{Ni}(p, p'x)$  at  $E_p = 120$  MeV. The total number of events is 4,000 for  $^{12}\text{C}$  target case while for  $^{58}\text{Ni}$  target case it is 14,000 for case-1  $\sigma_{NN}$  and 3,000 for case-2 and case-3  $\sigma_{NN}$ . As stated above, in the case of  $^{12}\text{C}$  target, we have used only case-1  $\sigma_{NN}$ . The data we compare with our calculations are taken from Ref. [33] and Ref. [34] for  $^{12}\text{C}$  and  $^{58}\text{Ni}$  targets, respectively. The range of the adopted impact parameter  $b$  is  $0 \leq b \leq 8$  fm in the case of  $^{12}\text{C}$  target, while  $0 \leq b \leq 10$  fm in the case of  $^{58}\text{Ni}$  target. If the incident proton comes out without making any two-nucleon collision, we regard that the event should not be included into inelastic scattering events to continuum. In the case of  $^{58}\text{Ni}$  target, we show in Fig. 2 the  $b$ -dependence of the probability  $P_{\text{n.col.}}(b)$  that the incident proton comes out without making any two-nucleon collision. It is to be noted that the total reaction cross section  $\sigma_R$  which we discuss later is calculated as

$$\sigma_R = \int_0^\infty 2\pi b db (1 - P_{\text{n.col.}}(b)). \quad (12)$$

The calculation of the double differential cross section  $d^2\sigma/d\Omega dE_{p'}$  is made in the following way;

$$\begin{aligned} \frac{d^2\sigma}{d\Omega dE_{p'}} &= \int_0^\infty 2\pi b db \frac{d^2\mathcal{N}(\mathbf{p}, b)}{d\Omega dE_{p'}}, \\ \frac{d^2\mathcal{N}(\mathbf{p}, b)}{d\Omega dE_{p'}} d\Omega dE_{p'} &= \left\langle \sum_{\substack{i=\text{isolated} \\ \text{protons}}} |\langle \mathbf{p} | \phi_{\mathbf{z}_i} \rangle|^2 \right\rangle_b d^3p, \\ |\langle \mathbf{p} | \phi_{\mathbf{z}_i} \rangle|^2 &= \left( \frac{1}{2\pi\hbar^2\nu} \right)^{3/2} \exp\left[ -\frac{1}{2\hbar^2\nu} (\mathbf{p} - \mathbf{K}_i)^2 \right] \end{aligned} \quad (13)$$

where  $d^3p = mp d\Omega dE_{p'}$ , and  $\langle \rangle_b$  stands for the average value over the events with impact parameter  $b$ . In this formula, the outgoing protons are expressed by Gaussian wave packets with momentum width  $\hbar\sqrt{\nu}$ . In the case of protons emitted during the dynamical stage, we adopt this width, but in the case of evaporated protons from a fragment of mass number  $A_F$ , we adopt narrower width by  $1/\sqrt{A_F}$ , namely  $\hbar\sqrt{\nu/A_F}$ . It is because the center-of-mass motion of the fragment of mass number  $A_F$  is described by a Gaussian wave packet whose momentum width is  $\hbar\sqrt{A_F\nu}$ , from which the standard deviation of momentum per nucleon is given by  $\hbar\sqrt{\nu/A_F}$ . In the actual calculation of the angular distribution, we further make another modification to  $|\langle \mathbf{p} | \phi_{\mathbf{z}_i} \rangle|^2$ . It is the cut of the high momentum tail of  $|\langle \mathbf{p} | \phi_{\mathbf{z}_i} \rangle|^2$ . The reason of this tail truncation is because the very high momentum part of the distribution  $|\langle \mathbf{p} | \phi_{\mathbf{z}_i} \rangle|^2$  has no physical justification. The tail part which we truncate is defined by the condition  $(\mathbf{p} - \mathbf{K}_i)^2/2\hbar^2\nu \geq 1.8^2$  for dynamical nucleons, and  $A_F(\mathbf{p} - \mathbf{K}_i)^2/2\hbar^2\nu \geq 1.8^2$  for evaporated nucleons. The volume of this tail part is about 10 % of the total volume of  $|\langle \mathbf{p} | \phi_{\mathbf{z}_i} \rangle|^2$ .

In Fig. 3 we give, in the case of the  $^{12}\text{C}$  target, the comparison of the calculated angular distribution  $d^2\sigma/d\Omega dE_{p'}$  with the data for various values of outgoing proton energy  $E_{p'}$ . We see that the reproduction of data is good. It is to be noted that good reproduction has been obtained without any adjustable parameter. In the case of  $E_p = 90$  MeV, the



cross sections at large angles for  $E_{p'} = 55$  and  $45$  MeV are under estimated. We think that the event number 4,000 is still not enough to reproduce large angle cross sections. From the study of  $^{58}\text{Ni}(p,p'x)$  shown in Fig. 6, we can guess that we need to increase the event number to about 10,000. In Figs. 4 and 5 we show the decomposition of the calculated angular distribution into multi-step contributions for the cases of  $E_p = 200$  and  $90$  MeV, respectively. We see that for our present region of  $E_{p'} \gtrsim 45$  MeV, the contribution of one-step process is predominant over a wide angular range but yet at large angles we can recognize some predominance of two-step process. Especially in the case of highly inelastic scattering with  $E_{p'} = 45$  MeV for  $E_p = 200$  MeV, the two-step process is dominant over a fairly wide angular range and is indispensable for the reproduction of data.

The comparison of the calculated angular distribution with the data in the case of the  $^{58}\text{Ni}$  target is given in Fig. 6. We see that the reproduction of data is again good in view of the absence of any adjustable parameter in our approach. What is to be noted here is the result that almost the same good reproduction of data is obtained for all three choices of in-medium cross section  $\sigma_{NN}$ , case-1  $\sigma_{NN}$ , case-2  $\sigma_{NN}$ , and case-3  $\sigma_{NN}$ . To state in more detail, case-1  $\sigma_{NN}$  gives slightly better data-fitting for  $E_{p'} = 100$  MeV, while case-3  $\sigma_{NN}$  gives somewhat better fitting for  $E_{p'} = 40$  MeV.

The decomposition into multi-step contributions of the calculated angular distribution is given in Fig. 7. The decomposition of the calculated angular distribution by case-2  $\sigma_{NN}$  is similar to that by case-3  $\sigma_{NN}$ . We see that two-step contribution is dominant at some large angle region and is indispensable for the reproduction of data. What is to be noted is the forward cross section in the case of highly inelastic scattering with  $E_{p'} = 40$  MeV. In this case the two-step contribution is much larger than the one-step contribution in the forward cross section in all the three cases of adopted in-medium  $\sigma_{NN}$ . It is because the quasi-free peak of the one-step process is located in fairly large angle region in the case of highly inelastic scattering. Another point to be noted is the contribution of three-step process in large angle region. Fig. 7 shows that in both cases of  $\sigma_{NN}$  the data points above  $\theta = 100^\circ$  for  $E_{p'} = 100$  MeV are reproduced mainly by three-step contributions. Also for  $E_{p'} = 60$  MeV, the data points above  $\theta = 120^\circ$  have large contributions from the three-step process. We clearly see that the two-step contribution is much more important in this case of  $^{58}\text{Ni}$  target than in the case of  $^{12}\text{C}$  target, which is of course quite natural.

In Fig. 7, we indicated with arrows ( $\alpha$ ) the angle of the quasi-free peak which is given by  $\cos^{-1} \sqrt{E_{p'}/E_p}$ . The peak angles of the calculated one-step angular distributions are however seen to be slightly shifted to forward direction. One of the reasons of this shift is the mean field effect. If the collision takes place at the point of the potential depth  $V$ , the angle of the quasi-free peak is given by  $\cos^{-1} \sqrt{(E_{p'} - V)/(E_p - V)}$ . When we take  $V = -50$  MeV, the shifts to forward direction of the angles of the quasi-free peak at  $E_{p'} = 100, 60,$  and  $40$  MeV are  $4^\circ, 9^\circ,$  and  $12^\circ$ , respectively. We show in Fig. 7 by arrows ( $\beta$ ) these shifted angles of the quasi-free peak obtained with  $V = -50$  MeV. We see that these shifted angles are now much closer to the peak angles of the calculated one-step angular distributions. Another possible reason of the angle shift is the refraction effect in the surface region of the target which makes the path of one-step nucleon bend to forward direction.

Recently Shinohara et al. [22] studied this reaction,  $^{58}\text{Ni}(p, p'x)$  at  $E_p = 120$  MeV, by the use of a semi-classical distorted wave model of nucleon inelastic scattering to continuum

[30–32]. Our angular distribution due to the one-step process is very similar to that of Ref. [22], while the two-step contribution of Ref. [22] is fairly larger than that of our calculation. Especially the bigger contribution of the two-step process than the one-step process seen in the case of  $E_{p'} = 60$  MeV in Ref. [22] is in disagreement with our result.

#### IV. DEPENDENCE ON IN-MEDIUM N-N CROSS SECTION

We have seen in the previous section that the calculated angular distribution  $d^2\sigma/d\Omega dE_{p'}$  of  $^{58}\text{Ni}(p, p'x)$  at  $E_p = 120$  MeV for  $E_{p'} \gtrsim 40$  MeV is insensitive to the choice of different in-medium cross section  $\sigma_{NN}$ . We investigate here the reason of it.

In Table II we show the calculated reaction cross section  $\sigma_R$  (Eq. (12)) by the use of case-1  $\sigma_{NN}$ , case-2  $\sigma_{NN}$ , and case-3  $\sigma_{NN}$ . We see clear difference between the values of  $\sigma_R$ 's obtained by different  $\sigma_{NN}$ . Reflecting the relation  $(\sigma_{NN})_{\text{case-1}} < (\sigma_{NN})_{\text{case-2}} < (\sigma_{NN})_{\text{case-3}}$ , the resulting  $\sigma_R$  satisfy  $(\sigma_R)_{\text{case-1}} < (\sigma_R)_{\text{case-2}} < (\sigma_R)_{\text{case-3}}$ . As is reflected in Eq. (12), the magnitude of  $\sigma_R$  is determined only by the magnitude of the cross section of the first collision of the incident proton. Namely the magnitude of  $\sigma_R$  does not reflect any information of the later reaction process after the first collision of the incident proton. On the other hand, the angular distribution for a fixed value of  $E_{p'}$  reflects not only first collision of the incident proton but also the reaction process after the first collision. Let us compare the reaction process due to  $(\sigma_{NN})_{\text{case-1}}$  with that due to  $(\sigma_{NN})_{\text{case-3}}$ . Since  $(\sigma_{NN})_{\text{case-3}}$  is larger than  $(\sigma_{NN})_{\text{case-1}}$ , the probability of the first collision by  $(\sigma_{NN})_{\text{case-3}}$  is higher than that by  $(\sigma_{NN})_{\text{case-1}}$ . But at the same time, the probability of the second and further collisions by  $(\sigma_{NN})_{\text{case-3}}$  is also higher than those by  $(\sigma_{NN})_{\text{case-1}}$ . Therefore the energy of the outgoing protons are much more damped in the average for  $(\sigma_{NN})_{\text{case-3}}$  than for  $(\sigma_{NN})_{\text{case-1}}$ . Thus the cross section  $d\sigma/dE_{p'}$  is not necessarily larger for  $(\sigma_{NN})_{\text{case-3}}$  than for  $(\sigma_{NN})_{\text{case-1}}$ , at the  $E_{p'}$  value where the one-step process makes large contributions. This compensation mechanism between the first-collision probability and the energy damping due to multiple collisions explains why the calculated angular distribution at fixed value of  $E_{p'}$  is almost independent of the in-medium N-N cross section within the present three kinds of  $\sigma_{NN}$ .

In Table II we have also shown the cross sections  $\sigma_{1\text{-step}}$  of outgoing protons due to the one-step process, for three cases of  $\sigma_{NN}$ . We see that  $\sigma_{1\text{-step}}$  is smaller for larger  $\sigma_{NN}$ . This result supports our above argument. If  $\sigma_{NN}$  is large, the nucleon after the first collision will make further collisions rather than escaping from the target without making further collisions. If this effect is bigger than the effect of the large cross section of the first collision,  $\sigma_{1\text{-step}}$  becomes smaller for larger  $\sigma_{NN}$ . Table II shows that it is actually the case.

The cross section  $\sigma_{\text{dyn}}$  in Table II is the cross section of dynamical protons, namely protons emitted during dynamical stage. We see that  $\sigma_{\text{dyn}}$  is not so much dependent on the magnitude of  $\sigma_{NN}$ . It is because the cross sections of protons due to higher multi-step processes tend to become larger for larger  $\sigma_{NN}$ , although  $\sigma_{1\text{-step}}$  is smaller for larger  $\sigma_{NN}$ .

In Table II we also give the calculated values of the cross sections  $\sigma_{\text{evap}}$  of evaporated protons. Quite naturally  $\sigma_{\text{evap}}$  is larger for larger  $\sigma_{NN}$ . The cross section  $\sigma_{p'}$  in Table II is the total cross section of all the outgoing protons, namely  $\sigma_{p'} = \sigma_{\text{evap}} + \sigma_{\text{dyn}}$ . The dependence of  $\sigma_{p'}$  on  $\sigma_{NN}$  is due to that of  $\sigma_{\text{evap}}$ .

In the approach with the semi-classical distorted wave model of Refs. [22,30–32], the

imaginary part  $W_{\text{opt}}$  of the optical potential and the in-medium cross section  $\sigma_{NN}$  are important ingredients of the model. These  $W_{\text{opt}}$  and  $\sigma_{NN}$  are mutually intimately related and hence the choice of these quantities should be made consistently. It means that the change of the magnitude of  $\sigma_{NN}$  needs to be made together with the consistent change of  $W_{\text{opt}}$ . On the other hand, in the case of our AMD approach, we need not to introduce  $W_{\text{opt}}$  and the role of  $W_{\text{opt}}$  is described automatically in the many-body dynamics which includes the two-nucleon collision process. Therefore when we change the  $\sigma_{NN}$  value in the AMD approach, it implies that such effects that are described by  $W_{\text{opt}}$  are changed consistently in an automatic way. This merit of the AMD approach is very advantageous in our present discussion of the dependence of  $d^2\sigma/d\Omega dE_{p'}$  on  $\sigma_{NN}$ . It is, however, to be noted that in principle there exists mutual relation between  $\sigma_{NN}$  and the effective nuclear force. Hence the change of  $\sigma_{NN}$  is to be correlated with the change of the effective nuclear force. In our present study we study the dependence of  $d^2\sigma/d\Omega dE_{p'}$  on  $\sigma_{NN}$  by assuming that the adoption of the Gogny force as the effective nuclear force is more reliable than the choice of  $\sigma_{NN}$ .

We have seen that the reaction cross section  $\sigma_R$  depends rather strongly on  $\sigma_{NN}$ . Therefore the comparison of the calculated  $\sigma_R$  with data is expected to give us important information on  $\sigma_{NN}$ . We here should recall that  $\sigma_R$  is determined by the cross section of the very first collision of the incident proton. Hence  $\sigma_{NN}$  which we expect to extract from  $\sigma_R$  data is that in the region of the incident energy  $E_p$ . To the knowledge of the present authors, the  $\sigma_R$  data of the  $^{58}\text{Ni} + \text{p}$  system at  $E_p = 120$  MeV are not available. However, as we discuss below, we have several reasons to expect that  $\sigma_R(^{58}\text{Ni}, 120 \text{ MeV})$  lies in the region of  $650 \sim 800$  mb. In Ref. [35] in which  $\sigma_R$  of  $^{40}\text{Ca} + \text{p}$ ,  $^{90}\text{Zr} + \text{p}$ , and  $^{208}\text{Pb} + \text{p}$  systems are experimentally studied in the wide energy range up to 200 MeV, we see that the approximate target-mass-number ( $A_T$ ) dependence and the approximate energy dependence of  $\sigma_R$  in all these three systems are  $\sigma_R \propto A_T^{2/3}$  and  $d\sigma_R/d\ln(E_p/\text{MeV}) \approx -170$  mb, respectively, in the region of  $50 \text{ MeV} \lesssim E_p \lesssim 150 \text{ MeV}$ . When we apply this empirical rule of  $A_T$  dependence to the data  $\sigma_R(^{40}\text{Ca}, 120 \text{ MeV})$  and  $\sigma_R(^{90}\text{Zr}, 120 \text{ MeV})$  given in Fig. 12 of Ref. [35], we get  $\sigma_R(^{58}\text{Ni}, 120 \text{ MeV}) \approx 750$  mb. According to Ref. [36], observed  $\sigma_R(^{58}\text{Ni})$  at  $E_p = 60.8$  MeV is 807 mb. When we apply the above empirical rule of energy dependence to this, we obtain  $\sigma_R(^{58}\text{Ni}, 120 \text{ MeV}) \approx 690$  mb. Furthermore in Ref. [36] it is reported that  $\sigma_R(^{59}\text{Co}) = 780$  mb at  $E_p = 98.5$  MeV and  $\sigma_R(\text{Cu}) = 751$  mb at  $E_p = 113$  MeV. All the above data and estimations support that  $\sigma_R(^{58}\text{Ni})$  at  $E_p = 120$  MeV is in the region of  $650 \sim 800$  mb. When we accept this range of value for  $\sigma_R(^{58}\text{Ni})$  at  $E_p = 120$  MeV, we can extract the conclusion that case-1  $\sigma_{NN}$  is most plausible in the region of  $E_p = 120$  MeV among the three cases of  $\sigma_{NN}$ , although case-1  $\sigma_{NN}$  gives still rather large  $\sigma_R$ .

In Fig. 6 we see that in the case of  $E_{p'} = 40$  MeV the calculated value of  $d^2\sigma/d\Omega dE_{p'}$  is smallest in the case of the case-3  $\sigma_{NN}$  than case-1 and case-2  $\sigma_{NN}$ . This makes the reproduction of the observed angular distribution by the case-3  $\sigma_{NN}$  slightly better than that by other  $\sigma_{NN}$ . Since the contribution of the one-step process is largest in the angle region around quasi-free peak, we can understand the situation as follows: In order for the proton with  $E_{p'} \approx 40$  MeV after the first collision to escape out of the target, this proton should not make second collision. If  $\sigma_{NN}$  is large, the probability to make the second collision is large and hence the value of  $d^2\sigma/d\Omega dE_{p'}$  due to one-step process becomes smaller. This argument implies that the in-medium cross section  $\sigma_{NN}$  in the low energy region around 40

MeV is better represented by the case-3  $\sigma_{NN}$  than other case-1 and case-2  $\sigma_{NN}$ . Namely,  $\sigma_{NN}$  in the low energy region around 40 MeV is suggested to be closer to the free cross section than case-1 and case-2  $\sigma_{NN}$ . But of course much more investigations are needed to have conclusive justification about this point.

## V. SUMMARY

Proton inelastic scatterings to continuum  $^{12}\text{C}(\text{p}, \text{p}'\text{x})$  at  $E_p = 200$  MeV and 90 MeV and  $^{58}\text{Ni}(\text{p}, \text{p}'\text{x})$  at  $E_p = 120$  MeV have been studied with AMD (antisymmetrized molecular dynamics) which has been successfully utilized for the study of heavy-ion collisions. Angular distributions  $d^2\sigma/d\Omega dE_{p'}$  for various  $E_{p'}$  energies have been shown to be reproduced well without any adjustable parameter. It shows the reliability and usefulness of AMD in describing light-ion reactions.

Decomposition of the calculated angular distributions into multi-step contributions has been made and two-step contributions have been found to be dominant in some large angle region and to be indispensable for the reproduction of data. In the case of highly inelastic scattering with  $E_{p'} = 40$  MeV of  $^{58}\text{Ni}(\text{p}, \text{p}'\text{x})$  at  $E_p = 120$  MeV, two-step contributions have been found to overwhelm one-step contributions in forward cross sections. Furthermore in the  $^{58}\text{Ni}(\text{p}, \text{p}'\text{x})$  case, even three-step processes have been found to make dominant contributions in the reproduction of data in the large angle region  $\theta \gtrsim 120^\circ$  for  $E_{p'} = 100$  MeV.

We have studied the dependence of the calculated angular distributions  $d^2\sigma/d\Omega dE_{p'}$  for various  $E_{p'}$  energies on the in-medium N-N cross section  $\sigma_{NN}$  in the case of  $^{58}\text{Ni}(\text{p}, \text{p}'\text{x})$  at  $E_p = 120$  MeV, and have found that the dependence is very weak. The reason of this insensitivity of  $d^2\sigma/d\Omega dE_{p'}$  to  $\sigma_{NN}$  has been clarified by studying also the  $\sigma_{NN}$ -dependence of various kinds of cross sections such as the reaction cross section  $\sigma_R$ , the one-step-proton cross section  $\sigma_{1\text{-step}}$ , and the evaporated-proton cross section  $\sigma_{\text{evap}}$ . Unlike  $d^2\sigma/d\Omega dE_{p'}$ , these quantities,  $\sigma_R$ ,  $\sigma_{1\text{-step}}$ , and  $\sigma_{\text{evap}}$ , have been shown to be sensitive to  $\sigma_{NN}$ . For the choice of larger  $\sigma_{NN}$ ,  $\sigma_R$  and  $\sigma_{\text{evap}}$  become larger, while  $\sigma_{1\text{-step}}$  becomes smaller for larger  $\sigma_{NN}$ .

## ACKNOWLEDGMENTS

The authors would like to thank Professors M. Kawai and Y. Watanabe for helpful discussions. Helpful comments of Professor D. Brink are gratefully acknowledged. They are also grateful to Professor H. Sakaguchi for helpful comments on experimental data. Their thanks are also due to Professors A. A. Cowley and J. J. Lawrie for kindly sending us detailed data values of  $^{12}\text{C}(\text{p}, \text{p}'\text{x})$  and  $^{58}\text{Ni}(\text{p}, \text{p}'\text{x})$ . They also would like to thank Miss S. Furihata for discussions about the calculation of the step numbers in the AMD study of  $^{12}\text{C}(\text{n}, \text{px})$  reactions. Numerical calculations were made mainly by using the Fujitsu VPP500 of RIKEN.

## REFERENCES

- [1] J. Griffin, Phys. Rev. Lett. **17**, 478 (1966); M. Blann, Annu. Rev. Nucl. Sci. **25**, 123 (1975); G. Mantzouranis, H. A. Weidenmüller, and D. Agassi, Z. Phys. **A276**, 145 (1976).
- [2] A. Iwamoto and K. Harada, Nucl. Phys. **A419**, 472 (1984).
- [3] H. Feshbach, A. Kerman, and S. Koonin, Ann. Phys. (N.Y.) **125**, 429 (1980).
- [4] T. Tamura, T. Udagawa, and H. Lenske, Phys. Rev. **C26**, 379 (1982).
- [5] H. Nishioka, H. A. Weidenmüller, and S. Yoshida, Ann. Phys. (N.Y.) **183**, 166 (1988); **193**, 195 (1989).
- [6] K. Kikuchi and M. Kawai, *Nuclear Matter and Nuclear Reactions* (North-Holland, Amsterdam, 1968)
- [7] M. L. Goldberger, Phys. Rev. **74**, 1269 (1948).
- [8] G.F.Bertsch and S.Das Gupta, Phys.Rep. **160**, 189 (1988).
- [9] J. Aichelin and H. Stöcker, Phys. Lett. **176B**, 14 (1986); J. Aichelin, Phys. Reports **202**, 233 (1991); G. Peilert, H. Stöcker, W. Greiner, A. Rosenhauer, A. Bohnet and J. Aichelin, Phys. Rev. **C39**, 1402 (1989).
- [10] D. H. Boal and J. N. Glosli, Phys. Rev. **C38**, 1870 (1988).
- [11] H. Horiuchi, Nucl. Phys. **A522**, 257c (1991).
- [12] A. Ono, H. Horiuchi, T. Maruyama, and A. Ohnishi, Phys. Rev. Letters **68** (1992), 2898; Prog. Theor. Phys. **87**, 1185 (1992).
- [13] A. Ono, H. Horiuchi, T. Maruyama, and A. Ohnishi, Phys. Rev. **C47**, 2652 (1993).
- [14] A. Ono, H. Horiuchi, and T. Maruyama, Phys. Rev. **C48**, 2946 (1993).
- [15] A. Ono and H. Horiuchi, to be published in Phys. Rev. **C**.
- [16] H. Horiuchi, *Proc. NATO Advanced Study Institute on Hot and Dense Nuclear Matter*, Bodrum (1993), eds. W. Greiner, H. Stöcker, and A. Gallmann, (Plenum, 1994), p.215.
- [17] H. Horiuchi, to appear in *Proc. Fifth Int. Conf. on Nucleus-Nucleus Collisions*, Taormina (1994).
- [18] H. Horiuchi, A. Ono, and Y. Kanada-En'yo, *Proc. Seventh Int. Conf. on Nuclear Reaction Mechanisms*, Varenna (1994), ed. E. Gadioli, p.421.
- [19] H. Horiuchi, T. Maruyama, A. Ohnishi, and S. Yamaguchi, *Proc. Int. Conf. on Nuclear and Atomic Clusters*, Turku (1991), eds. M. Brenner, T. Lönnroth, and F. B. Malik, (Springer, 1992), p.512; *Proc. Int. Symp. on Structure and Reactions of Unstable Nuclei*, Niigata (1991), eds. K. Ikeda and Y. Suzuki, (World Scientific, 1992), p.108.
- [20] Y. Kanada-En'yo and H. Horiuchi, Prog. Theor. Phys. **93** No.1 (1995).
- [21] H. Horiuchi, Y. Kanada-En'yo, and A. Ono, *Proc. Second Int. Conf. on Atomic and Nuclear Clusters*, Santorini (1993), eds. G. S. Anagnostatos and W. von Oertzen, Z. Phys. **A349**, 279 (1994).
- [22] H. Shinohara, Y. Watanabe, and M. Kawai, preprint KU-ECE(NS)-94-01
- [23] M. Saraceno, P. Kramer, and F. Fernandez, Nucl. Phys. **A405**, 88 (1983).
- [24] H. Feldmeier, Nucl. Phys. **A515**, 147 (1990); *Proc. NATO Advanced Study Institute on the Nuclear Equation of State*, Peñíscola(1989), eds. W. Greiner and H. Stöcker, (Plenum, 1989), p.375.
- [25] S. Drożdż, J. Okolowicz, and M. Ploszajczak, Phys. Lett. **109B**, 145 (1982); E. Caurier,

- B. Grammaticos and T. Sami, Phys. Lett. **109B**, 150 (1982); W. Bauhoff, E. Caurier, B. Grammaticos and M. Ploszajczak, Phys. Rev. **C32**, 1915 (1985).
- [26] T. Maruyama, A. Ono, A. Ohnishi, and H. Horiuchi, Prog. Theor. Phys. **87**, 1367 (1992).
- [27] F. Pühlhofer, Nucl. Phys. **A280**, 267 (1977).
- [28] J. Dechargé and D. Gogny, Phys. Rev. **C43**, 1568 (1980).
- [29] H. W. Bertini, Oak Ridge National Laboratory Report No. ORNL-3383 (1963).
- [30] Y. L. Luo and M. Kawai, Phys. Lett. **B235**, 211 (1990); Phys. Rev. **C43**, 2367 (1991).
- [31] M. Kawai and H. A. Weidenmüller, Phys. Rev. **C45**, 1856 (1992).
- [32] Y. Watanabe and M. Kawai, Nucl. Phys. **A560**, 43 (1993).
- [33] S. V. Förtsch, A. A. Cowley, J. V. Pilcher, D. M. Whittal, J. J. Lawrie, J. C. Van Staden, and E. Friedland, Nucl. Phys. **A485**, 258 (1988).
- [34] S. V. Förtsch, A. A. Cowley, J. J. Lawrie, D. M. Whittal, J. V. Pilcher, and F. D. Smit, Phys. Rev. **C43**, 691 (1991).
- [35] A. Nadasen, P. Schwandt, P. P. Singh, W. W. Jacobs, A. D. Bacher, P. T. Debevec, M. D. Kaitchuck, and J. T. Meek, Phys. Rev. **C23**, 1023 (1981).
- [36] W. Bauhoff, Atomic Data and Nuclear Data Tables, **35**, No.3, 434 (1986).

FIGURES

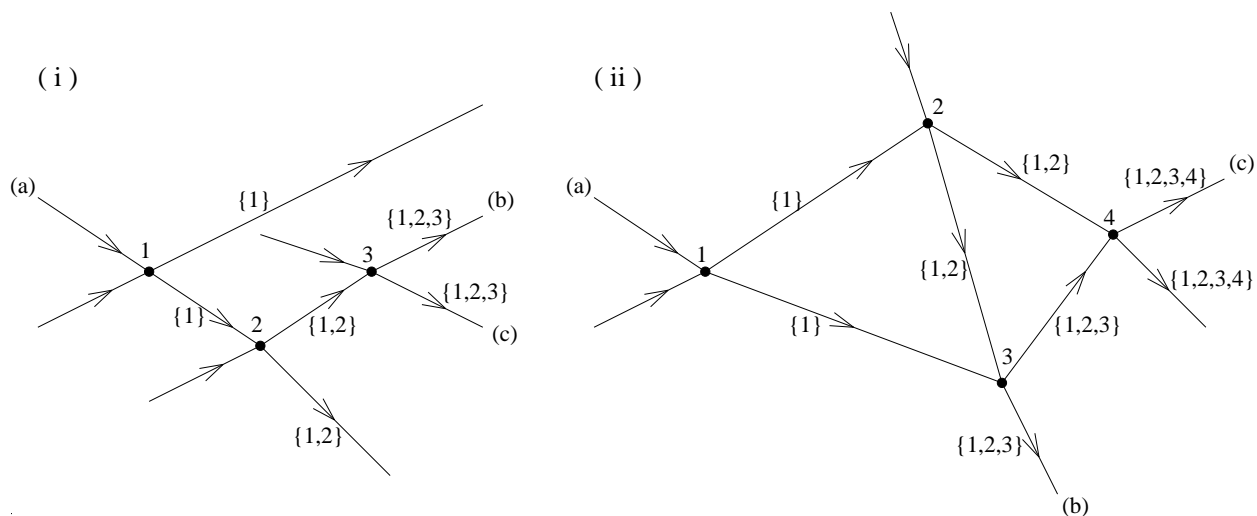


FIG. 1. Illustrative examples of multi-step process. Nucleon (a) is the incident proton and collision points are labeled by collision indices 1, 2, ... instead of No.1, No.2, .... In the figure (i), the outcoming nucleons (b) and (c) carry the same set of collision indices  $\{1, 2, 3\}$  and hence are three-step nucleons. In the figure (ii), the exit nucleon (b) is a three-step nucleon since it carries a set  $\{1, 2, 3\}$  composed of three collision indices, while the exit nucleon (c) carrying a set  $\{1, 2, 3, 4\}$  is a four-step nucleon.

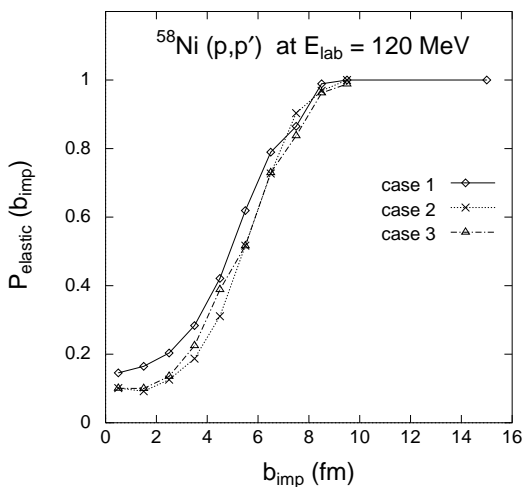


FIG. 2. Impact-parameter ( $b$ ) dependence of the probability  $P_{\text{n.col}}$  that the incident proton comes out without making any two-nucleon collision. Calculations are made for  $^{58}\text{Ni}(p, p'x)$  at  $E_p = 120$  MeV by the use of three kinds of in-medium N-N cross section  $\sigma_{NN}$  explained in the text.

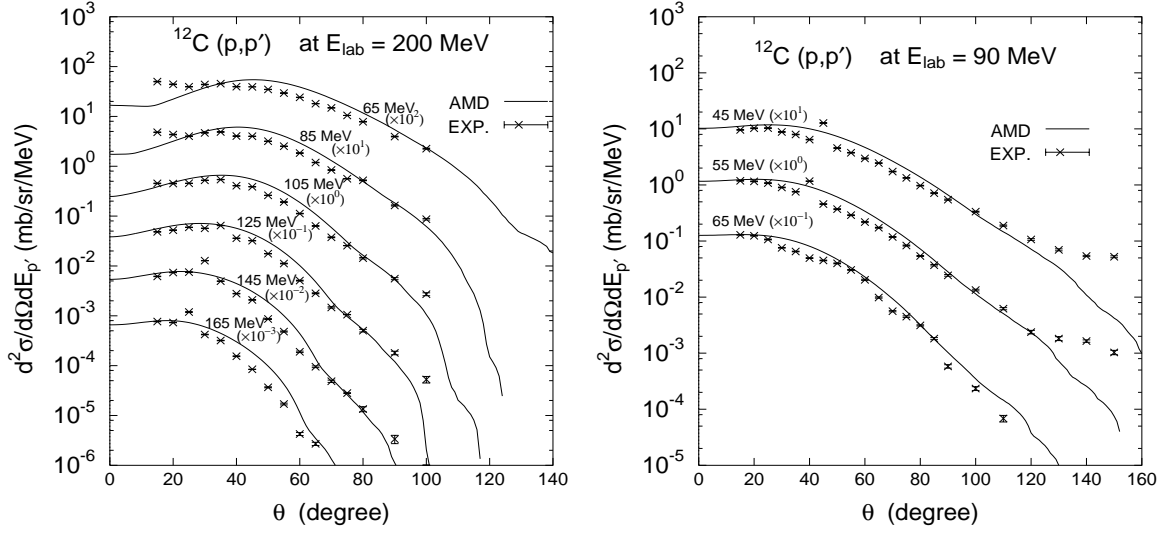


FIG. 3. Comparison of calculated angular distribution  $d^2\sigma/d\Omega dE_{p'}$  of  $^{12}\text{C}(p, p')$  with data for various  $E_{p'}$  energies. Comparisons are made in two cases of incident proton energies  $E_p = 200$  MeV and 90 MeV.

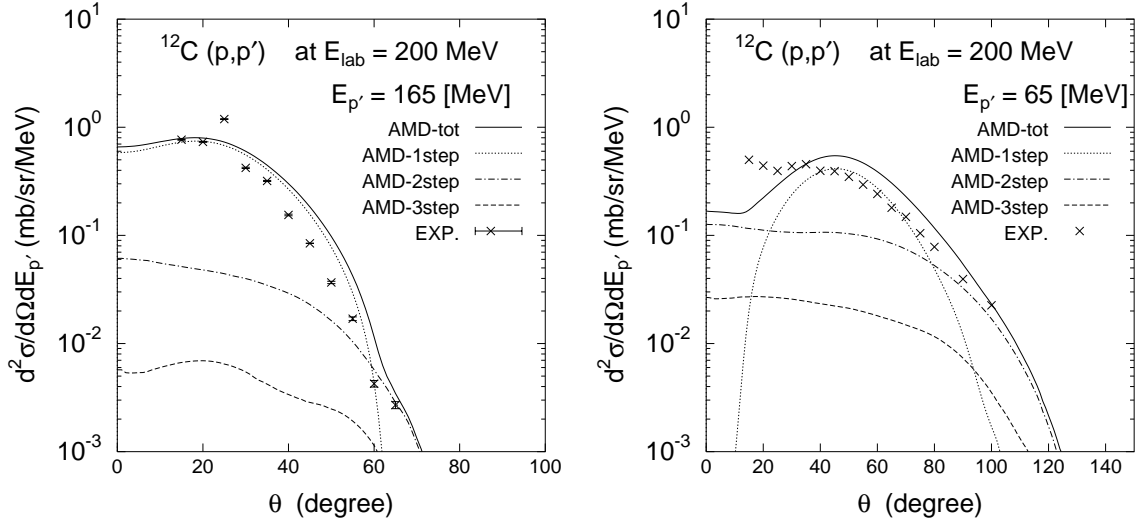


FIG. 4. Decomposition of the calculated angular distributions into multi-step contributions in the case of  $^{12}\text{C}(p, p')$  at  $E_p = 200$  MeV.



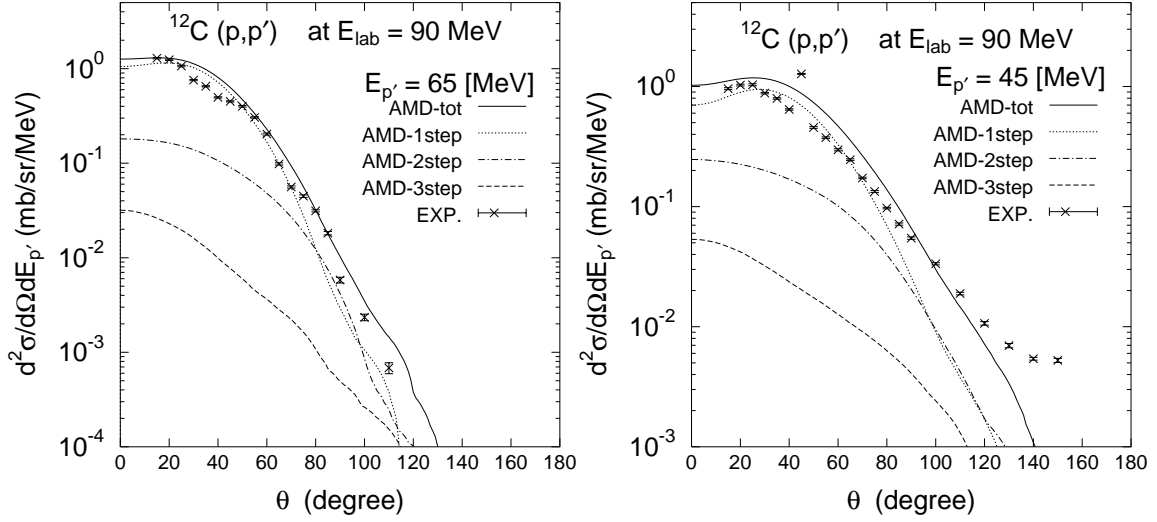


FIG. 5. Decomposition of the calculated angular distributions into multi-step contributions in the case of  $^{12}\text{C}(p, p')$  at  $E_p = 90$  MeV.

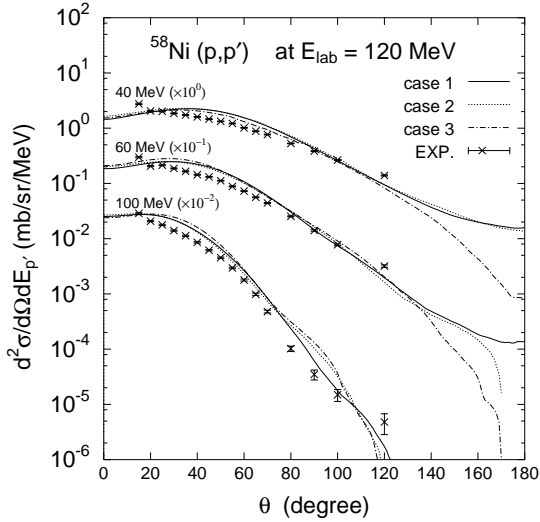


FIG. 6. Comparison with data of calculated angular distribution  $d^2\sigma/d\Omega dE_{p'}$  of  $^{58}\text{Ni}(p, p')$  with incident proton energy  $E_p = 120$  MeV. Comparisons are made for three kinds of calculations performed by adopting three different in-medium N-N cross sections; case-1  $\sigma_{NN}$ , case-2  $\sigma_{NN}$ , and case-3  $\sigma_{NN}$ .

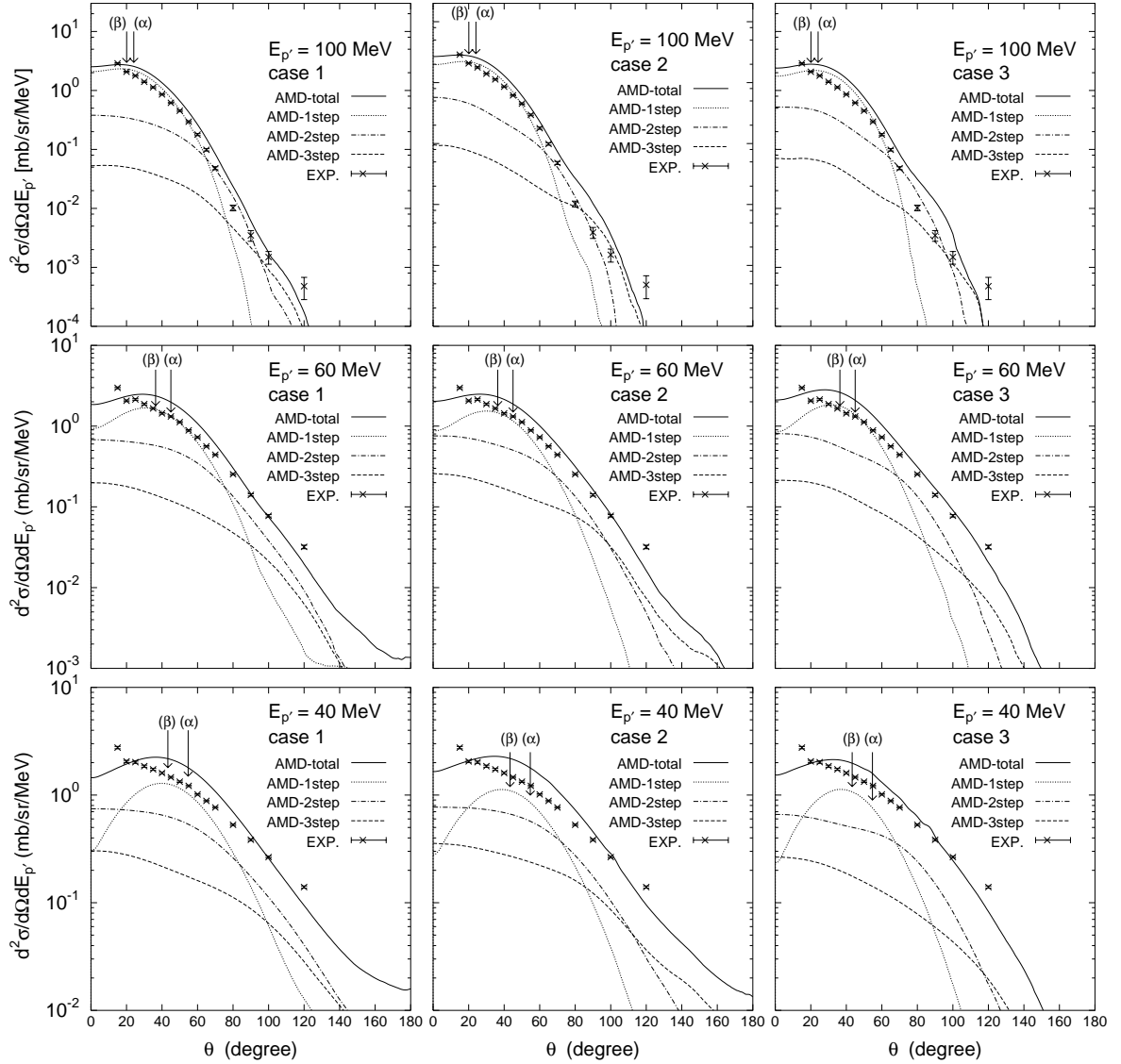


FIG. 7. Decomposition of the calculated angular distributions of  $^{58}\text{Ni}(p, p'x)$  at  $E_p = 120$  MeV into multi-step contributions. The angles indicated with arrows  $(\alpha)$  and  $(\beta)$  are quasi-free scattering angles given by  $\cos^{-1} \sqrt{E_{p'}/E_p}$  and  $\cos^{-1} \sqrt{(E_{p'} - V)/(E_p - V)}$  with  $V = -50$  MeV, respectively.

TABLES

TABLE I. Values of parameters  $A_1(E)$ ,  $B_1(E)$ , and  $B_2(E)$  in mb/sr as functions of the incident particle laboratory energy  $E$ , used in the parametrization of the angular distribution of  $\sigma_{pn}$  of the case-3  $\sigma_{NN}$  which is taken from Ref. [29]. See Eq. (10).

$E$ (MeV)	$A_1(E)$	$B_1(E)$	$B_2(E)$
40	12.0	7.0	7.0
80	5.2	8.1	8.3
120	3.3	6.6	9.0
160	2.3	3.9	7.7
200	2.0	3.6	6.5
240	1.9	3.6	6.2
280	1.8	3.6	6.0

TABLE II. Dependence of various kinds of cross sections on the different choices of in-medium N-N cross section  $\sigma_{NN}$ , case-1  $\sim$  case-3. The notations  $\sigma_R$ ,  $\sigma_{1\text{-step}}$ ,  $\sigma_{\text{dyn}}$ ,  $\sigma_{p'}$ , and  $\sigma_{\text{evap}}$  stand for the reaction cross section, the one-step-proton cross section, the dynamical-proton cross section, the total-proton cross section, and the evaporated-proton cross section, respectively. Units are in mb.

	case-1	case-2	case-3
a ) $\sigma_R$	839	965	973
b ) $\sigma_{1\text{-step}}$	589	518	489
c ) $\sigma_{\text{dyn}}$	1027	1079	994
d ) $\sigma_{p'}$	1749	2259	2308
e ) $\sigma_{\text{evap}}$	722	1180	1314